

Sodium VCHP with Carbon-Carbon Radiator for Radioisotope Stirling Systems

Calin Tarau^a, William G. Anderson^a, William O. Miller^b, and Rogelio Ramirez^b

^a*Advanced Cooling Technologies, Inc., 1046 New Holland Ave., Lancaster, PA 17601
717-295-6104, Bill.Anderson@1-act.com*

^b*Allcomp, Inc., 209 Puente Avenue, City of Industry, CA 91746*

Abstract. In a Stirling radioisotope system, heat must continually be removed from the General Purpose Heat Source (GPHS) modules to maintain the modules and surrounding insulation at acceptable temperatures. The Stirling converter normally provides this cooling. If the Stirling converter stops in the current system the insulation is designed to spoil, preventing damage to the GPHS at the cost of an earlier termination of the mission. An alkali-metal Variable Conductance Heat Pipe (VCHP) can be used to allow multiple stops and restarts of the Stirling converter. A sodium VCHP with a Haynes 230 envelope was designed and fabricated for the Advanced Stirling Radioisotope Generator (ASRG), with a baseline 850°C heater head temperature. When the Stirling converter is stopped, the heat from the GPHS is rejected to the Cold Side Adapter Flange using a low-mass, carbon-carbon radiator. The VCHP is designed to activate with a ΔT of 30°C. The 880°C temperature when the Stirling converter is stopped is high enough to avoid risking standard ASRG operation, but low enough to save most of the heater head life. The VCHP has low mass and low thermal losses for normal operation. The design has been modified from an earlier, stainless steel prototype with a nickel radiator. In addition to replacing the nickel radiator with a low mass carbon-carbon radiator, the radiator location has been moved from the ASRG case to the cold side adapter flange. This flange already removes two-thirds of the heat during normal operation, so it is optimized to transfer heat to the case. The VCHP was successfully tested with a turn-on ΔT of 30°C in three orientations: horizontal, gravity-aided, and against gravity.

Keywords: Variable Conductance Heat Pipe, Carbon-Carbon Radiator, Radioisotope Stirling System, Advanced Stirling Radioisotope Generator

PACS: 44.30.+v, 44.35.+c

INTRODUCTION

In the Advanced Stirling Radioisotope Generator (ASRG), two General Purpose Heat Source (GPHS) modules supply heat to dual Stirling converters (Stirling engine with an integrated linear alternator) (Chan, Wood, and Schreiber, 2007). This heat is used to generate electric power, while the waste heat is radiated to space. The maximum allowable GPHS module operating temperature is set by the iridium cladding around the fuel. The GPHS module is designed so that it will not release radioisotopes, even under such postulated events as a launch vehicle explosion, or reentry through the earth's atmosphere. However, if the iridium cladding was to overheat, grain boundary growth could weaken the cladding, possibly allowing radioisotopes to be released during an accident. Once the GPHS is installed in the radioisotope Stirling system, it must be continually cooled. Normally, the Stirling converter removes the heat, keeping the GPHS modules cool. There are three basic times when it may be desirable to stop and restart the Stirling converter:

1. During installation of the GPHS
2. During some missions when taking scientific measurements to minimize electromagnetic interference and vibration
3. Any unexpected stoppage of the converter during operation on the ground or during a mission.

In the current system design, the insulation spoils (partially melts) if the convertor stops, to protect the GPHS from overheating. A VCHP would allow convertor operation to be restarted on a planned convertor stoppage and potentially allow for convertor restart on any unexpected stoppage, depending on the reason for the stoppage. It would also save replacing the insulation after such an event during ground testing.

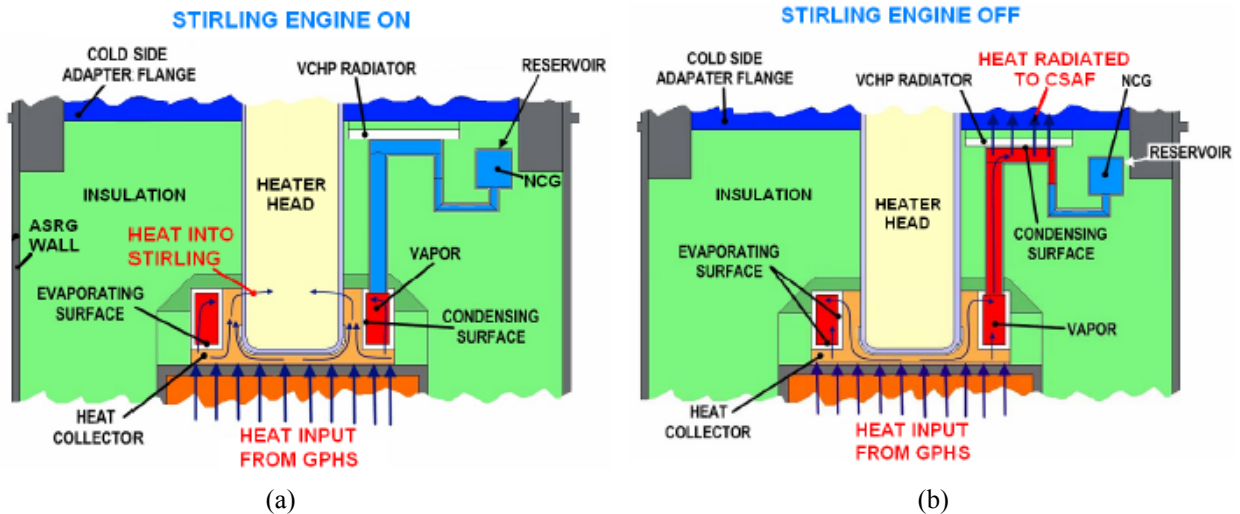


FIGURE 1. a) VCHP delivers heat to the heater head when the Stirling engine is working. b) VCHP dumps heat to the radiator when the Stirling engine is stopped.

The schematics in Fig. 1 show the basic concept of the VCHP integrated with a Stirling convertor. A GPHS module supplies heat to the heat collector which, in turn, wraps around the hot end of the Stirling convertor’s heater head, so the normal heat flow path is GPHS – heat collector – heater head. The annular evaporator of the VCHP wraps around the heat collector so, during normal operation, vapor is approximately at the heater head’s temperature. The non-condensable gas (NCG) charge in the system is sized so the radiator is blocked during normal operation (see Fig. 1(a)). When the Stirling engine is stopped, the temperature of the entire system starts to increase. Since the system is saturated, the working fluid vapor pressure increases as the temperature increases. This compresses the NCG. As shown in Fig. 1b, this opens up the radiator. Once the radiator is fully open, all of the heat is dumped to the radiator, and the temperature stabilizes. Once the Stirling engine starts operating again, the vapor temperature and pressure start to drop. The non-condensable gas blankets the radiator, and the system is back to the normal state (Fig. 1(a)).

The Advanced Stirling Radioisotope Generator (ASRG) (Chan, Wood, and Schreiber, 2007) was selected as the baseline Stirling system design. The system consists of two Advanced Stirling Convertors (ASCs), mounted back to back to minimize vibration. Heat to each ASC is supplied by one GPHS module. A cold-side adapter flange, shown in Figure 1 is used to conduct the waste heat from the Stirling engine cold side to the ASRG housing. This is fabricated from copper, and serves as a structural member. As shown in Figure 1, when the Stirling convertor is turned off, then the radiator dumps all of the heat from the GPHS to the Cold Side Adapter Flange (CSAF).

TABLE 1. VCHP Design Requirements.

GPHS Power (W)	250
GPHS Power to the Stirling Engine (W)	225
Heater Head Temperature (°C)	850
Heater Head Material	Mar-M 247
Conduction Losses down the Heater Head Wall (W)	6.5
Heat Collector Material (Baseline)	Nickel 201
Potential Reservoir Location	Cold-Side Adapter Flange
Cold-Side Adapter Flange Temp. (°C)	40 to 120
Heat Pipe Working Fluid	Sodium or NaK
VCHP Temperature when Stirling is Off (°C)	880

A summary of the design requirements is presented in Table 1. The heater head hot-end temperature was assumed to be 850°C for this program, compared to the current ASRG engineering unit temperature of 650°C. To accommodate this increase, the heater head material was changed from the current Inconel 718 to Mar-M 247. Mar-M 247 is a nickel-based casting alloy designed to have good tensile and creep rupture properties at elevated temperatures.

Earlier, a first prototype VCHP was fabricated to demonstrate the concept. To reduce costs, the main body was fabricated from stainless steel 304 and the radiator from nickel. The radiator in the first prototype rejected the waste heat to the ASRG wall, rather than the CSAF. The prototype successfully operated at temperatures up to 790°C, turning on with a 30°C ΔT . Details of the first prototype design and testing can be found in Tarau, Anderson, and Walker (2009).

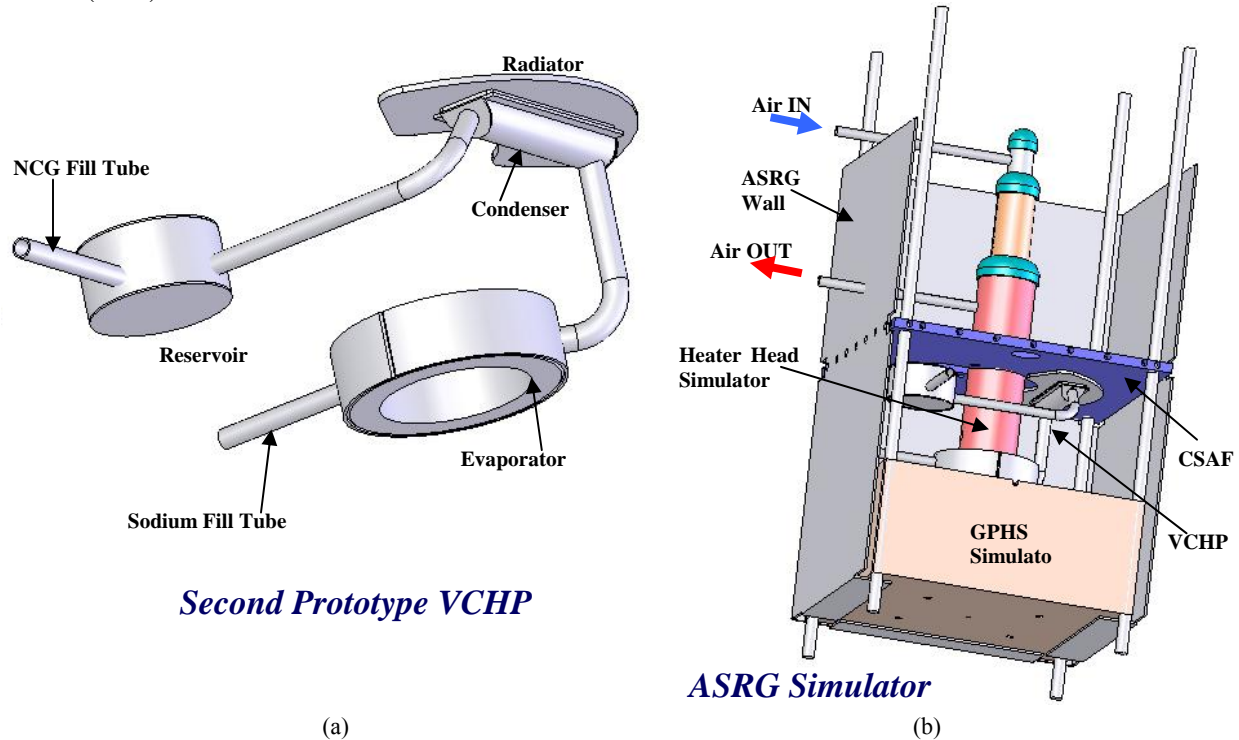


FIGURE 2. In the second prototype, the radiator dumps heat to the Cold Side Adapter Flange. (a) VCHP. (b) Schematic of the VCHP installed in the test system.

SECOND PROTOTYPE DESIGN

The second prototype design is shown in Figure 2. Changes to the design from the first prototype include:

- Replacing the nickel radiator with a low-mass carbon-carbon radiator
- Using Haynes 230 to fabricate the heat pipe envelope
- Moving the radiator so that heat is rejected to the CSAF, rather than the ASRG case
- Moving the reservoir so that excess heat entering the reservoir when the Stirling convertor is off is also rejected to the CSAF.

The radiator mass is significantly reduced by using a carbon-carbon radiator, due to both the lower density and higher thermal conductivity. Haynes 230 was selected as the envelope material because of both its compatibility with sodium based on long duration life tests (Rosenfeld et. al. 2004) and its low creep rate at 850°C. The screen wick structure was still 304 stainless steel, since no structural loads are applied to the wick.

The advantages of moving the radiator to face the CSAF include:

- The CSAF is always warmer than the ASRG wall. Consequently, heat leaks decrease during normal operation (ASC ON), and the condenser can be warmer preventing the working fluid (sodium) from freezing.
- The entire VCHP is more compact. The gravity head is decreased, reducing the screen wick thickness, and reducing the mass
- Rejecting the heat to the CSAF rather than to the ASRG wall makes the VCHP independent of the ASRG housing architecture. This advantage makes the back-up cooling system (VCHP) more general and suitable for other radioisotope based energy conversion systems.
- Moving the reservoir closer to the CSAF simplifies the thermal design of the reservoir.

The second prototype VCHP is shown in Figure 3 from two view angles. The heater head simulator (stainless steel 304) uses compressed air for cooling to simulate heat removal from the Stirling convertor heater head. It is structurally similar to the one used in the first prototype and presented in Tarau et al. 2009. It is welded to the nickel 201 heat collector as a leak tight assembly. The heat is now radiated to the CSAF by the 3D C-C radiator, conducted to the ASRG simulator walls (Figure 2), and further radiated into the environment (vacuum chamber wall) by the ASRG simulator walls. The reservoir also radiates some heat to the CSAF (~1.5 W) to maintain its low temperature. The evaporator wraps around the heat collector and is brazed (1100°C) to it using Amdry 105. The VCHP has two fill tubes: one attached to the evaporator and used for the main charge of sodium (it was pinched after charging) and another one attached to the reservoir and used for NCG charge and VCHP tuning (having a semi-permanent valve on its end). Both the evaporator and the reservoir have thermo-wells for vapor intrusive temperature measurements.

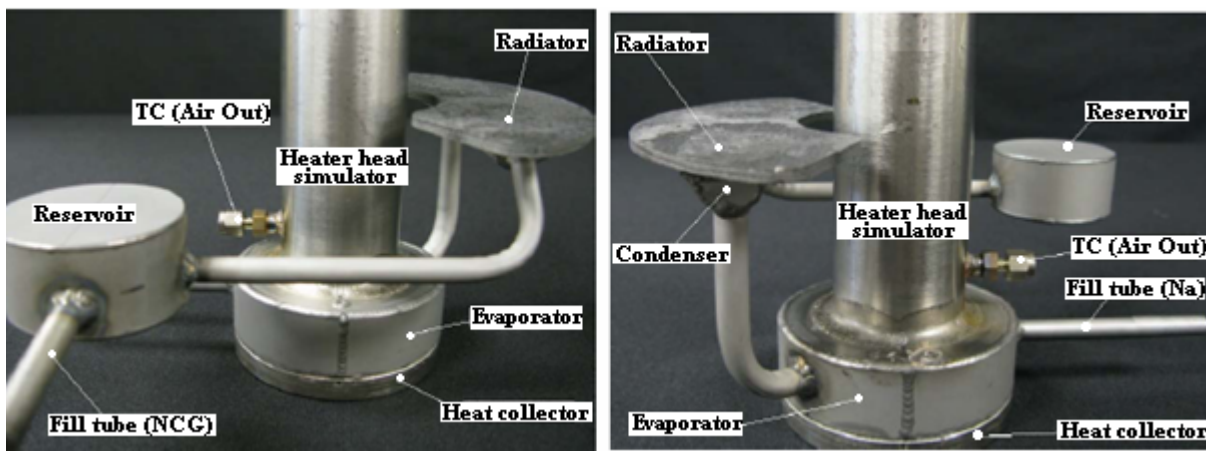


FIGURE 3. Two views of the second prototype VCHP

The “D” shaped condenser is brazed to the 3D C-C radiator through the flat surface and using a 2mm thick POCO Foam interface to mitigate the C.T.E mismatch between the Haynes 230 condenser and 3D C-C radiator panel. Figure 4 shows the 3D C-C radiator panel attached to the condenser where following parts can be identified:

- 3D Carbon-Carbon (C-C) radiator panel (2 mm thick)
- POCO Foam interface (2 mm thick)
- Condenser shell (Haynes 230, 15.5mm OD, 0.889mm wall thickness)
- Condenser back plate (Haynes230, 1mm thick)
- VCHP evaporator-condenser connecting tube (Haynes 230, 8mm OD)
- VCHP condenser-reservoir connecting tube (Haynes 230, 6.35mm OD)

The total mass is roughly 257 g. The masses are estimated because the heat collector and portions of the heater head simulator are attached to the VCHP before fabrication is complete, so the VCHP cannot be weighed.

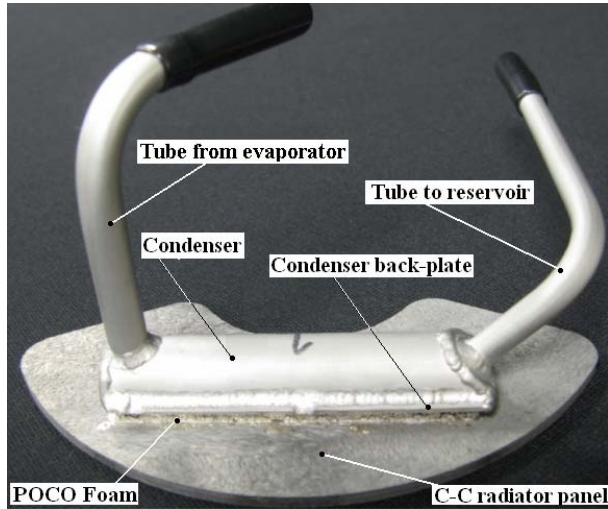


FIGURE 4. 3D C-C radiator panel – condenser assembly for the second prototype

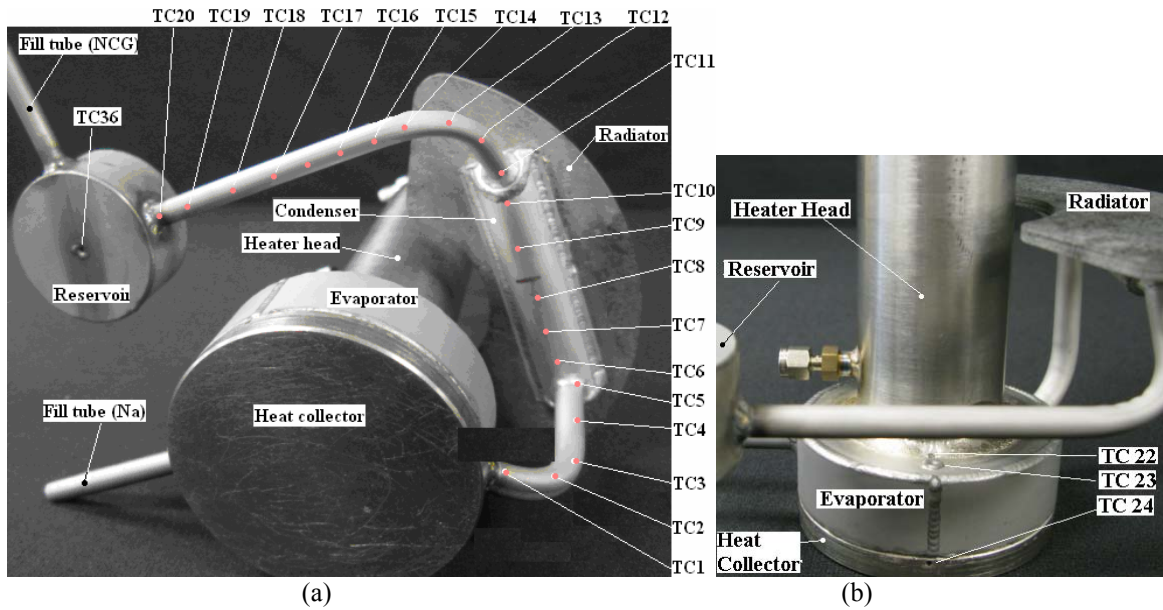


FIGURE 5. Thermocouple locations in the second prototype. (a) all the TCs except 22, 23 and 24 (b) TCs 22, 23 and 24.

Figure 5 shows the locations of the thermocouples used to measure the temperature distribution along the VCHP. Most of the thermocouples were spot welded to the pipe except thermocouples 22, 23, 24 and 36. Thermocouples 23 and 36 were installed into Haynes 230 thermo-wells to intrusively measure the vapor temperature in the evaporator (TC 23) and NCG temperature in the reservoir (TC 33). Thermocouples 22 and 24 measured the temperatures within the heat collector at locations adjacent to the evaporation interface (TC 24) and to the condensation interface, between the heater head and evaporator (TC 23). Condenser temperatures were measured by thermocouples 6 through 10. The remaining thermocouples, shown in Figure 5 (a), measured temperature distributions along the evaporator-condenser connecting tube (thermocouples 1 through 5) and condenser-reservoir connecting tube (thermocouples 11 through 20). The average distance between the thermocouple locations is approximately 12 mm. All these thermocouple locations will be relevant later in this paper where the results are discussed. The VCHP was charged with 17 cm³ of sodium. The NCG (argon) charge was varied for each normal operation point (heater head and vapor temperature) the system was tested for. An amount of 4.98×10^{-4} moles of NCG was used for the baseline vapor temperature of 850°C.

Carbon-Carbon Radiator

A carbon-carbon (C-C) laminate radiator was developed by Allcomp, Inc. for the second prototype. In addition to reducing the mass, the required radiator size can be reduced, due to the higher thermal conductivity of the carbon-carbon, compared to the previous nickel radiator. The radiator joint design had to minimize the thermal stresses between the Haynes 230 and the carbon-carbon radiator.

Whereas the properties of C-C remain essentially constant over this temperature domain, Haynes 230 varies somewhat. The thermal expansion coefficient of carbon-carbon ($\sim 4\text{ppm}/^\circ\text{C}$) is quite low in comparison to Haynes 230; in addition, its strength is lower. Haynes 230's C.T.E and Young's modulus both change with increasing temperature, but in an inverse manner. From room temperature to 1000°C , the C.T.E is reported to increase 30%, while its modulus decreases by roughly the same amount. The reduction in stiffness helps reduce the thermal stresses during brazing, but the increase in C.T.E. provides an offsetting influence. It is possible this trend continues out to the braze point; one could hope that a softening in modulus would increase more rapidly than a C.T.E increase. Nonetheless, for the design analysis we chose to assume constant properties for both. A braze temperature was set at $\sim 1200^\circ\text{C}$ to provide an operational margin, and a nickel-silicon alloy (Nicrobraz 30) was chosen being well suited to this goal.

Allcomp has a history of successfully joining C-C to super-alloys and titanium using CuSil ABA at 815°C . Since this application involved a significant increase in temperature range, a brazing test program was undertaken to explore joint issues. The initial test specimens involved joining several composite materials to Inconel tubing. Inconel was chosen because of its availability and reasonable C.T.E match to Haynes 230. Figure 6 depicts three braze specimen configurations from the latter series that evaluated joining of different materials at 1190°C with Nicrobraz. One may note that symmetry was utilized to eliminate bending stresses. For the POCO foam to tube (b) and 3 D CC to tube (c) stress at the interface joint is compressive and with some shear. Joining of the 2D CC to POCO foam (a) was a well C.T.E matched pair.

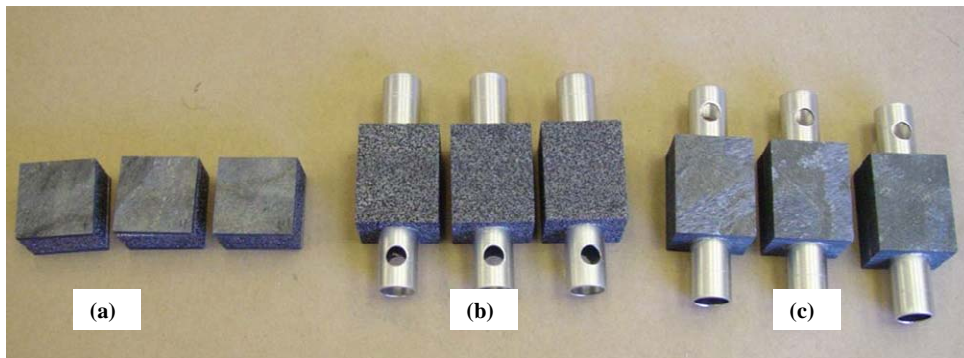


FIGURE 6. Photograph of three types of Nicrobraz 30 braze specimens, (a) 2D C-C to POCO Foam, (b) POCO Foam to Inconel tubing, and (c) direct brazing of 3D CC to POCO Foam.

Figure 7 is a close-up of the brazed joint of POCO Foam to Inconel tube. No cracks were observed. This POCO foam has been processed by Allcomp to enhance its strength. The Allcomp POCO foam density was $0.8\text{g}/\text{cc}$ and its measured compressive strength is 18.26MPa (2650psi), approximately 18 times the compressive strength measured for virgin POCO foam at $0.5\text{g}/\text{cc}$. The corresponding tensile strength was measured to be 10.1MPa (1470psi) at $0.8\text{g}/\text{cc}$.

Direct brazing of 3D CC to Inconel tube, without an interface material to moderate thermally induced stresses, resulted in one small crack near the braze interface (Figure 8). The interlaminar strength of the 3D CC under this severe condition was able to resist the imposed shear load for the most part. However, direct joining of the 3D CC was not in serious contention, but a test of its interlaminar strength in a high stress situation was of interest. Realizing that the interlaminar shear and compressive strength of the 3D CC panel would be limiting, a compliant layer of the Allcomp-processed POCO foam was placed between the panel and condenser wall. It is worth noting that the unit is nearly stress-free while operating. Stress fractures are caused by induced stresses upon returning to room temperature.

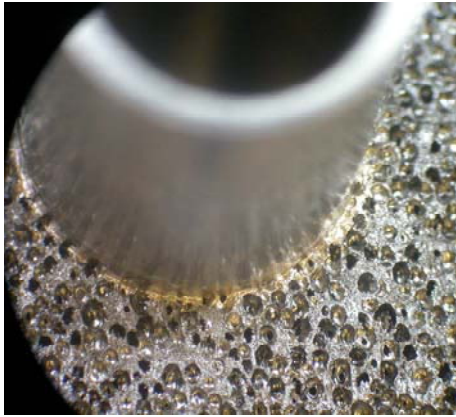


FIGURE 7. Photographic view of the braze joint of POCO foam to Inconel tubing..

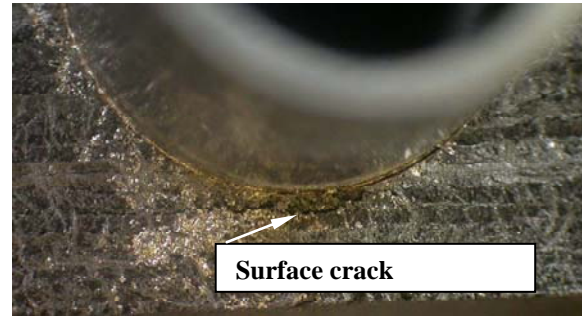


FIGURE 8. Photograph of crack in 3D CC at braze interface of C-C directly to Inconel tube.

As the final design evolved it became clear that the approach chosen for the compact, lightweight structure was a single-sided radiator mounted on a half-shell. This configuration change introduced a bending stress from asymmetry between the metal structure and the radiator panel. Also, the half-shell and flat closure plate presented unknown distortion effects during cool-down from brazing. It remained to be shown through actual construction whether the POCO foam tensile strength properties would adequately handle the increased stress. Prototype brazing results (Figure 7) indicated that the compressive strength of the Allcomp modified POCO foam was adequate.

The approach taken to resolve the tensile stress was to study the benefit of increased POCO foam material thickness, utilizing both FEA and full-scale prototyping. The location of the foam material placed between the 3D CC material and the flat condenser closure plate is shown in Figure 9.

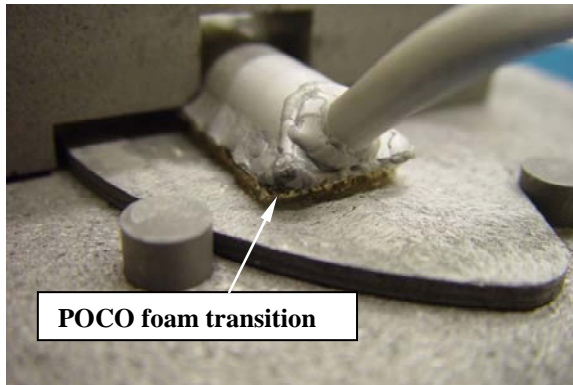


FIGURE 9. Photograph of the VCHP condenser and CC radiator panel in graphite braze fixture.



FIGURE 10. Photograph of the final brazed structure with 8mm thick POCO foam transition member.

A FEA model with non-linear material properties was used to predict the three dimensional POCO Foam stress field. It was judged that reasonable agreement between this model and the braze result was obtained, since tensile stress cracks which were observed at the very end of the POCO foam were also indicated by the virtue that the ultimate tensile stress was exceeded. The FEA also predicted that increasing the Foam thickness would reduce this induced stress somewhat. The final prototype assembly is shown in Figure 10.

Four brazed full-scaled prototypes were produced. The results of this prototype effort clearly showed that brazing a single-sided 3D CC radiator panel to a compact Haynes 230 condenser was practical. To a large extent all aspects of the design were realized. However, small tensile surface cracks at the extreme ends of the POCO foam remained, in spite of changing from 2mm to 8mm thickness. Based on our FEA analysis this minor cracking could be overcome by increased POCO foam tensile strength. Processing the POCO foam to a higher tensile strength may

allow a less thick POCO foam piece. Our estimate suggests that doubling its tensile strength to 20MPa (2,900psi) would provide an adequate stress margin.

EXPERIMENTAL SETUP

The VCHP integrated with the GPHS and ASRG simulators is shown in Fig. 11a. The GPHS simulator uses a MoSi_2 spiral heater (rated to work at 1400°C continuously), which radiantly heats the bottom of the heat collector. Because of the high temperature of the heater during the Stirling stoppage ($\sim 1100^\circ\text{C}$), the heater and its ceramic base are directly encased by a $\frac{1}{2}$ " thick Duraboard 3000 insulation. However, the bulk insulation material is Microtherm board that in turn, encases the Duraboard 3000 envelope. Microtherm board is rated for temperatures up to 1000°C with an average thermal conductivity of 0.025 W/mK . As mentioned above, heat removal by the Stirling converter is simulated by a steady flow of air through the annular space of the heater head simulator. The ASRG walls are simulated by copper plates with a 1.6 mm thickness to match thermal resistance of the ASRG beryllium walls.

Figure 11b shows the ASRG simulator test setup ready for preliminary tests in the vacuum chamber. Two copper tubes connect the air IN and OUT ports of the heater head with the feed through flange of the vacuum chamber. The flexibility of these copper tubes allows testing of the ASRG simulator in any orientation inside the vacuum chamber. A Pitot tube is installed outside of the vacuum chamber on the "Air IN" line to measure the air velocity. The following parameters are monitored beside the temperature profiles along the VCHP:

- CSAF temperature
- ASRG Wall temperatures
- Vacuum chamber wall temperature
- Heater head simulator temperatures
- Heater temperature
- Air IN and OUT temperatures
- Air velocity (using a pitot tube)
- Electrical power

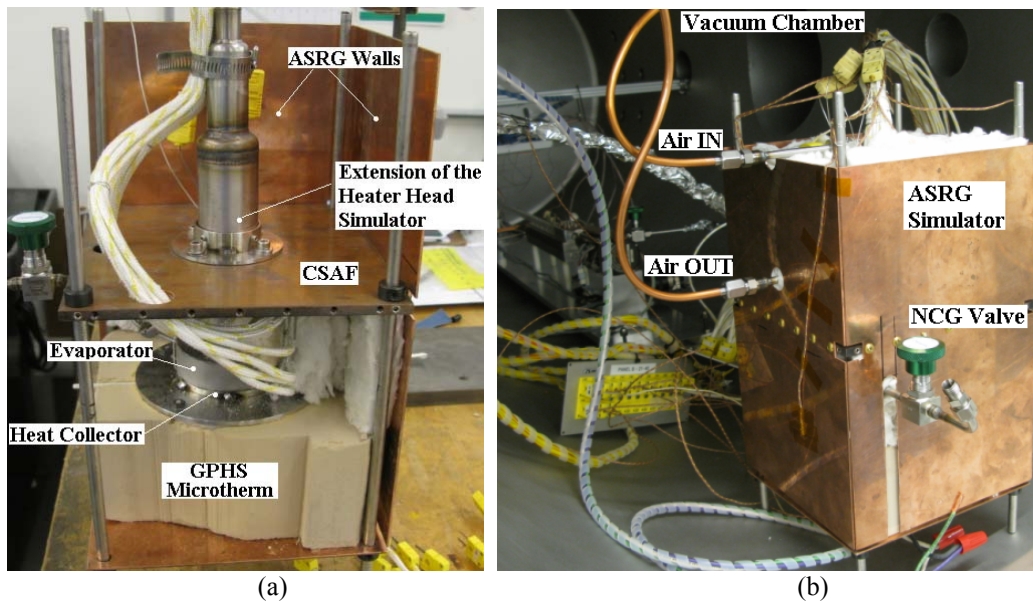


FIGURE 11. Experimental setup (a) Integration of the VCHP with the GPHS and ASRG simulators (b) Experimental setup in vacuum chamber.

RESULTS

The second prototype was tested for three nominal vapor temperatures, 775°C, 790°C and 850°C under both extreme orientations, gravity aided and against gravity. In addition, the system was tested in the horizontal orientation with an 850°C vapor temperature. Because the results for the 775°C and 790°C vapor temperature cases were similar to the 850°C case, only the results for 850°C are presented since this is the nominal working temperature of the ASRG. Table 2 below summarizes relevant parameters measured during the 850°C vapor temperature case. The parameters presented are electrical power applied to the heater, reservoir temperature, condenser temperature (TC 8), CSAF temperature, ASRG wall temperature (average), heater temperature and vacuum chamber wall temperature (average). These parameters are obtained for the three orientations presented in the first column of Table 2 and explicitly shown in Fig. 12. Numbers 1, 2 and 3 in the second line of Table 2 refer to the experimental context for each orientation. Each context is described below:

Context 1: Heat Losses The system is supplied with the minimum electrical power to maintain a vapor temperature of 850°C under steady state conditions. No cooling is applied during this context and the applied power compensates for all of the heat losses.

Context 2: ASC “ON”, VCHP “OFF” The system is supplied with the total electrical power consisted of the two components: losses and nominal heat input to the ASC (~225W). However, note that in all three orientations the total power was higher than the heat losses and the nominal heat input, since the radiator is oversized. In Context 2, cooling is applied (simulating a working ASC) to maintain a vapor temperature of 850°C, with the front at the exit of the evaporator (between TC 23 and TC 1). This context simulates normal operation of the ASRG, before the ASC stoppage, when the VCHP is OFF.

Context 3: ASC “OFF”, VCHP “ON” The system is continuously supplied with the same total power as Context 2, while no cooling is applied. This context simulates the system after the ASC is stopped and VCHP is turning ON, rejecting the heat through the radiator to the CSAF under steady state conditions.

Table 2. Relevant system parameters during measurements at 850°C nominal vapor temperature.

Orientation	Power [W]		Reservoir Temp.[°C]			Condenser Temp.[°C]		CSAF Temp.[°C]			ASRG Wall Temp.[°C]			Heater Temp.[°C]			Chamber Wall Temp.[°C]		
	1	2	1	2	3	1	2	1	2	3	1	2	3	1	2	3	1	2	3
Against Gravity	169	448	245	248	305	299	315	108	112	196	92	95	148	948	1066	1090	32	33	40
Gravity Aided	178	448	247	261	310	310	303	103	119	205	87	103	155	950	1066	1088	29	34	41
Horizontal	166	438	248	268	321	292	303	105	123	199	92	111	153	945	1047	1079	25	31	35

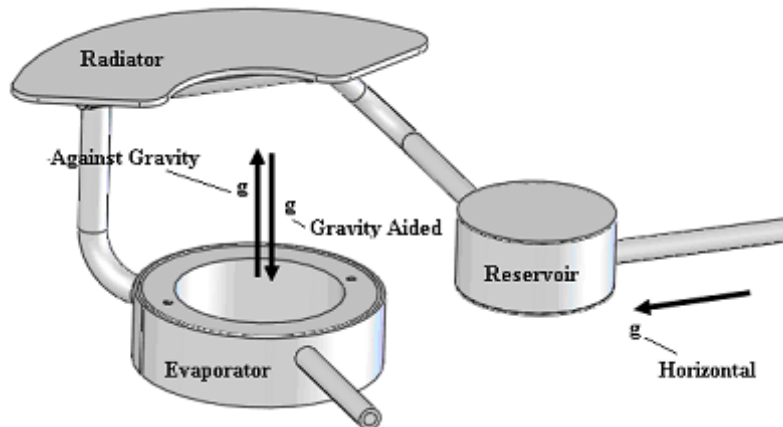


FIGURE 12. The directions of gravity corresponding to the three orientations of the VCHP during testing.

The transient VCHP temperature profiles for the gravity aided case are presented in Figures 13 and 14. In Fig. 13, the front travels from the evaporator to the condenser as a result of the ASC stoppage. The first temperature profile (ASC ON before stoppage) corresponds to Context 2. At this point the cooling air is active and the evaporator is at 850°C (TC 23), and all of the heat is traveling from the heater, through the annular evaporator to the heater head simulator and into the cooling air. The radiator is OFF, with condenser temperatures around 310°C.

Once cooling is stopped (ASC OFF), the system starts to heat up, and the NCG gas front moves toward the condenser. As it travels up the condenser, heat is radiated to the CSAF, conducted to the ASRG copper walls and then radiated to the ambient (vacuum chamber walls). The sequence shown in Fig. 13 starts with Context 2 and ends with Context 3 when the front has settled to fully open the condenser. It can be observed that reservoir temperature increased from 261°C to 310°C while the vapor temperature (TC 23) increased with the prescribed $\Delta T=30^\circ\text{C}$. Also, several thermocouples after TC 23 (which is the reference being intrusive in the vapor) show higher values than TC 23 itself. These thermocouples (1, 2, and 3) are close enough to the heat collector to sense higher temperatures than the inside environment because of the heat traveling through the pipe walls driven by the higher temperature heat collector. In fact, during this sequence, the approximately first inch of the evaporator–condenser connecting tube becomes an extension of the evaporator. This trend reverses as we go further from the heat collector along the VCHP tube.

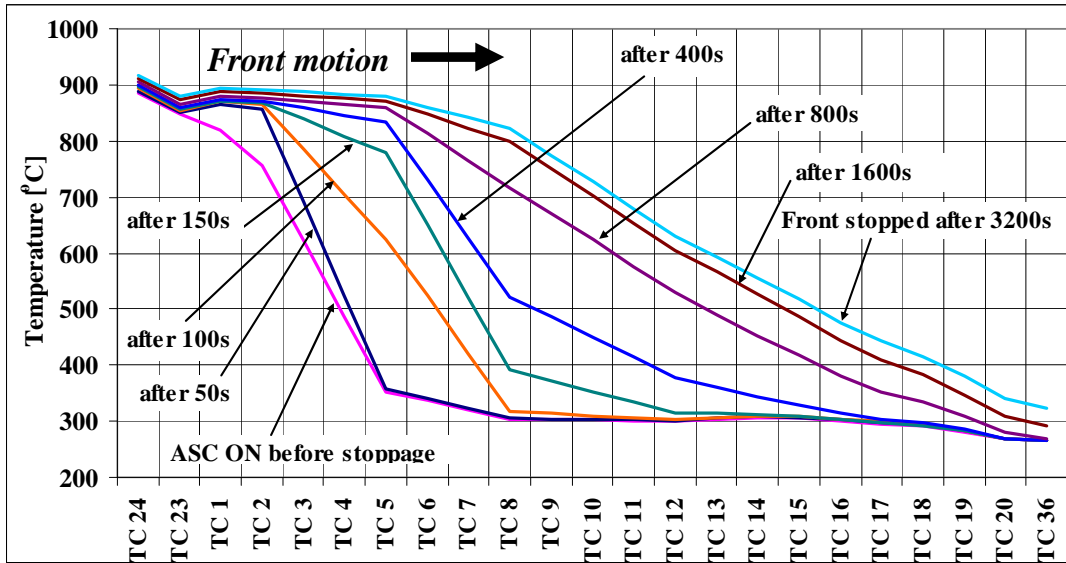


FIGURE 13. VCHP temperature distributions when the simulated ASC is initially ON and the VCHP orientation is “Gravity Aided?”. After the simulated convertor is turned OFF, the front moves toward the end of the condenser to turn the VCHP ON.

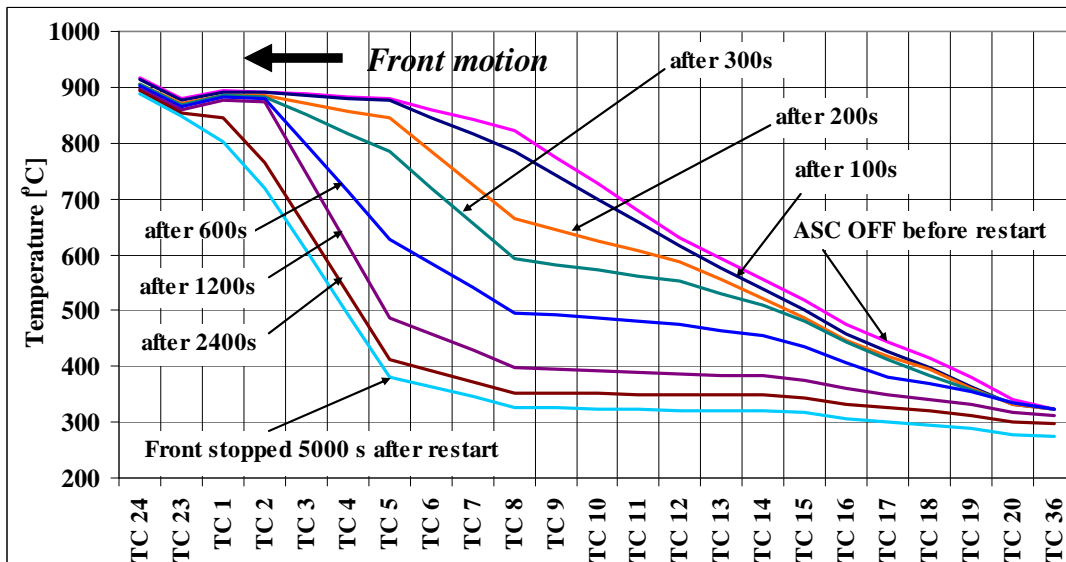


FIGURE 14. VCHP temperature distributions when the simulated ASC is initially OFF and the VCHP orientation is “Gravity Aided?”. After the simulated convertor is turned ON, the front retracts toward the evaporator to turn the VCHP OFF.

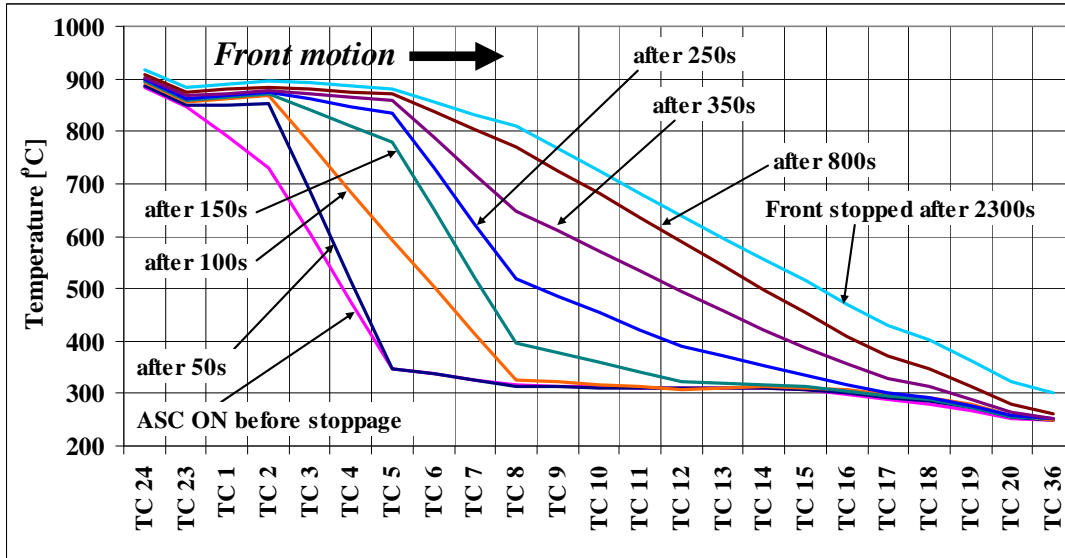


FIGURE 15. VCHP temperature distributions when the simulated ASC is initially ON and the VCHP orientation is “Against Gravity”. After the simulated convertor is turned OFF, the front moves toward the end of the condenser to turn the VCHP ON.

The sequence shown in Fig. 14 refers to the restarting the cooling air, turning OFF the VCHP. It starts with Context 3, then the cooling is turned ON (ASC starts working). The heat is again absorbed by the heater head simulator and vapor cools down, allowing the front to travel back to the evaporator. Normally, this sequence ends with Context 2. However, steady states were difficult to be reached since they take a very long time. The moments when a steady state was considered as reached were arbitrarily chosen throughout the entire experiment, mostly using the vapor temperature (TC 23) as a reference. Taking these facts into account, some inconsistencies regarding the parameters in Table 2 may be this way explained. Also, temperature profile in Fig. 14 that is shown as the steady state after ASC was restarted shows significant differences compared to Context 2 and especially the reservoir and condenser temperatures that are now slightly higher.

Although a non relevant parameter for VCHP operation in the actual ASRG system, the transient response of the front was evaluated. Approximately 3200s were needed by the VCHP to turn ON and 5000s to turn OFF during the “Gravity Aided” experiment.

The results of the “Against Gravity” orientation case are presented in Figures 15 and 16. The experiment was carried under similar conditions as the “Gravity Aided” orientation case. No significant differences were observed especially from VCHP performance point of view. However, slightly lower condenser and reservoir temperatures are noticed. Also the heat losses during Context 1 are lower for the “Against Gravity” case. The traveling times of the front are now 2300s for the VCHP turning ON and 2800s for VCHP turning OFF, showing a faster transient response of the front in the “Against Gravity” case. All these results are consistent with the observations made on the first prototype. These temperatures, power loss and transient response differences were attributed to both external natural convection and internal buoyancy forces that, in the “Gravity Aided” case, heated the condenser and the reservoir more earlier compared to the “Against Gravity” case. In the presented case (the second prototype), natural convection is removed from the scenario so the internal buoyancy forces remain as the only explanation. As mentioned, to confirm this theory, horizontal measurements were carried out for the position shown in Fig. 12.

In the horizontal orientation, approximately 2200s were needed by the VCHP to turn ON and 3800s to turn OFF. These transient responses are within a certain extent consistent with the previous cases, especially the VCHP turning OFF time. However, the VCHP turning ON time is slightly faster than in the “Against Gravity” case which was unexpected. The unusual VCHP configuration and the fact that only one from the four positions that can be labeled as “horizontal orientation” was investigated, may play a role in the occurrence of these inconsistencies.

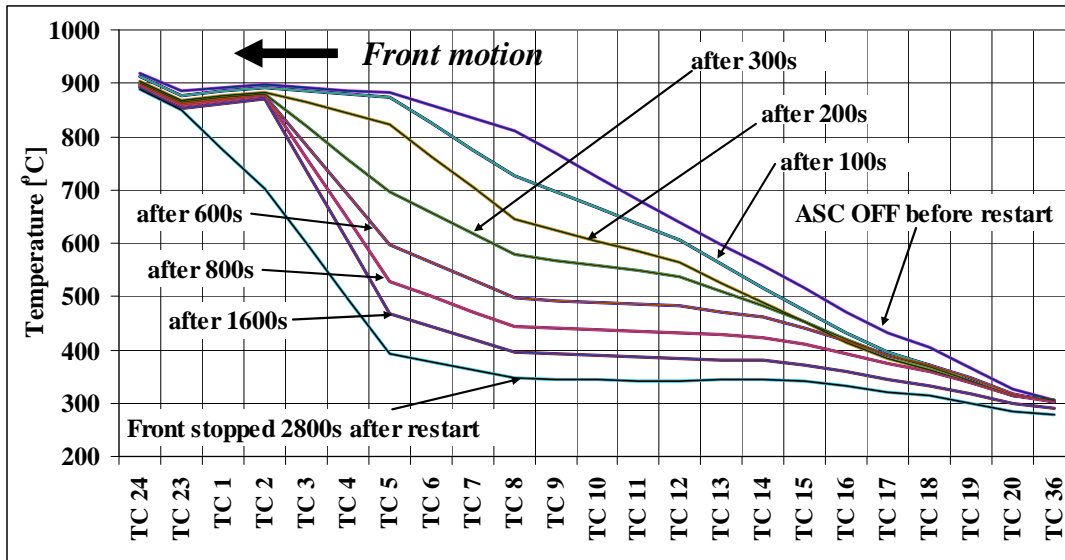


FIGURE 16. VCHP temperature distributions when the simulated ASC is initially OFF and the VCHP orientation is “Against Gravity”. After the simulated convertor is turned ON, the front retracts toward the evaporator to turn the VCHP OFF.

FUTURE WORK

A third (final) prototype is currently being fabricated. It is an improved version of the second prototype presented in this paper. One of the major improvements is heat leak reduction. Heat leaks induced by the heater head simulator will be reduced by using shorter and thinner walls for the heater head simulator. Heat leaks through the VCHP itself when ASC is ON and VCHP is OFF will be reduced by using a thinner wick structure in the VCHP tubes. This is a key consideration for the overall VCHP design and integration within the ASRG. General heat leaks will be reduced by using a thinner and smaller GPHS flange, better insulation using Microtherm and a better brazing quality of the evaporator to the heat collector. A new C-C Radiator with better brazing will be also an improvement for the final prototype. Unlike for the second prototype, TCs will be inserted in both C-C panel and POCO Foam interface for both better evaluation of the heat losses caused by the VCHP and better characterization of the C-C – POCO Foam – Condenser interface.

CONCLUSIONS

The second VCHP prototype for a radioisotope Stirling system has been successfully fabricated and tested. The second prototype was entirely fabricated from Haynes 230 with a carbon-carbon radiator. An ASRG simulator was used to test the VCHP in the vacuum chamber as relevant environment. The system has a baseline temperature of 850°C and uses sodium as the working fluid. The experimental results matched the modeling predictions very well for both “gravity aided” and “against gravity” (upside down) working conditions. “Horizontal” measurements were performed as well. For the “gravity aided” case and under steady conditions, the front was located at the evaporator exit with a vapor temperature of 850°C for the simulated case of an operating Stirling convertor (cooling was active and the VCHP was OFF). When the cooling was stopped (simulating a stopped Stirling convertor), the gas front moved and settled at the end of the condenser with a 880°C vapor temperature and turning on the VCHP. This showed a 30°C vapor temperature increase, as designed. When cooling was started again (simulating a restart of the Stirling convertor), the gas front retreated to the evaporator exit to turn off VCHP radiator. The VCHP settled at the same vapor temperature as the initial, 850°C. The VCHP performance was similar for the “against gravity” case. Heat rejected by the radiator was about 270 W for both “gravity aided” and “against gravity” cases. Heat leaks for the overall apparatus were approximately 160-175 W.

The only noticeable difference between the results of the two extreme cases (“gravity aided” and “against gravity”), was the front traveling time. The reservoir was slightly hotter in the “gravity aided” case than in the

“against gravity” case during both cold (VCHP OFF) and hot (VCHP ON) regimes. In the “against gravity” case the front traveling speed was approximately 20% slower than for the “gravity aided case”. Previous tests in air with the first prototype had a much larger difference in transient time, with the “gravity aided” system taking roughly twice as long to reach steady state. The hypothesis is that the difference in the reservoir temperatures and their transients determines the difference in front velocity between the two cases. In addition, the gravity effects may cause the reservoir temperature differences. Internal buoyancy forces on the sodium vapor, which is lighter than the NCG (argon) at the reservoir temperature, may heat the reservoir more in the “gravity aided” case. External natural convection also heated the reservoir during tests in air with the first prototype. The findings in the second prototype confirm this hypothesis. First the difference between the front speeds was just 20%, compared to 100% difference in the first prototype when natural convection was active. Measurements in the horizontal position are also consistent, with a front speed intermediate between the “gravity aided” and “against gravity” experiments.

ACRONYMS

ASRG - Advanced Stirling Radioisotope Generator	GPHS - General Purpose Heat Source
3D - Three Dimensional	NCG - Non Condensable Gas
C-C - Carbon-Carbon	TC - Thermocouple
CSAF - Cold Side Adapter Flange	VCHP - Variable Conductance Heat Pipe

ACKNOWLEDGMENTS

This research was sponsored by NASA Glenn Research Center under Phase II Small Business Innovation Research (SBIR) Contract No. NNC07QA40P. Any opinions, findings, and conclusions or recommendations expressed in this article are those of the authors and do not necessarily reflect the views of the National Aeronautics and Space Administration. Lanny Thieme is the contract technical monitor. We would like to thank John Hartenstine of Advanced Cooling Technologies, Inc., Jeff Schreiber and Jim Sanzi of NASA Glenn Research Center, Wei Shih of Allcomp, Inc., and Jaime Reyes, Jack Chan, and Michael Welz of Lockheed Martin Space Systems Company for helpful discussions about the Stirling system and the VCHP. Tim Wagner was the technician for the program.

REFERENCES

- Chan, T.S., Wood, J. G. and Schreiber, J. G., “Development of Advanced Stirling Radioisotope Generator for Space Exploration,” NASA Glenn Technical Memorandum NASA/TM-2007-214806, 2007. <http://gltrs.grc.nasa.gov/reports/2007/TM-2007-214806.pdf>.
- Rosenfeld, J. H., Ernst, D. M., Lindemuth, J. E., Sanzi, J., Geng, S. M., and Zuo, J., “An Overview of Long Duration Sodium Heat Pipe Tests,” NASA Glenn Technical Memorandum NASA/TM—2004-212959, 2004. <http://gltrs.grc.nasa.gov/citations/all/tm-2004-212959.html>.
- Tarau, C., Anderson, W. G., and Walker, K. L., “Sodium Variable Conductance Heat Pipe for Radioisotope Stirling Systems,” IECEC 2009, Denver, CO, Aug. 2 – 5, 2009.